

# The effects of flagellar hook compliance on motility of monotrichous bacteria: A modeling study

Cite as: Phys. Fluids 24, 061901 (2012); <https://doi.org/10.1063/1.4721416>

Submitted: 30 November 2011 . Accepted: 30 April 2012 . Published Online: 08 June 2012

H. Shum, and E. A. Gaffney



View Online



Export Citation

## ARTICLES YOU MAY BE INTERESTED IN

[Dynamics of swimming bacteria at complex interfaces](#)

Physics of Fluids 26, 071902 (2014); <https://doi.org/10.1063/1.4887255>

[Life at low Reynolds number](#)

American Journal of Physics 45, 3 (1977); <https://doi.org/10.1119/1.10903>

[Choice of computational method for swimming and pumping with nonslender helical filaments at low Reynolds number](#)

Physics of Fluids 28, 021901 (2016); <https://doi.org/10.1063/1.4940904>



## The effects of flagellar hook compliance on motility of monotrichous bacteria: A modeling study

H. Shum<sup>a)</sup> and E. A. Gaffney

*Centre for Mathematical Biology, Mathematical Institute, University of Oxford,  
24–29 St. Giles', Oxford OX1 3LB, United Kingdom*

(Received 30 November 2011; accepted 30 April 2012; published online 8 June 2012)

A crucial structure in the motility of flagellated bacteria is the hook, which connects the flagellum filament to the motor in the cell body. Early mathematical models of swimming bacteria assume that the helically shaped flagellum rotates rigidly about its axis, which coincides with the axis of the cell body. Motivated by evidence that the hook is much more flexible than the rest of the flagellum, we develop a new model that allows a naturally straight hook to bend. Hook dynamics are based on the Kirchhoff rod model, which is combined with a boundary element method for solving viscous interactions between the bacterium and the surrounding fluid. For swimming in unbounded fluid, we find good support for using a rigid model since the hook reaches an equilibrium configuration within several revolutions of the motor. However, for effective swimming, there are constraints on the hook stiffness relative to the scale set by the product of the motor torque with the hook length. When the hook is too flexible, its shape cannot be maintained and large deformations and stresses build up. When the hook is too rigid, the flagellum does not align with the cell body axis and the cell “wobbles” with little net forward motion. We also examine the attraction of swimmers to no-slip surfaces and find that the tendency to swim steadily close to a surface can be very sensitive to the combination of the hook rigidity and the precise shape of the cell and flagellum. © 2012 American Institute of Physics. [<http://dx.doi.org/10.1063/1.4721416>]

### I. INTRODUCTION

Propulsion of flagellated micro-organisms has been the subject of mathematical analysis for over half a century. The earliest work of Taylor<sup>1</sup> described swimming due to waves propagating along an infinite two-dimensional sheet but this quickly developed into new approaches for solving the fluid mechanical problem of long filaments moving in viscous media, namely, resistive force theory (RFT) (Ref. 2) and slender body theory (SBT).<sup>3</sup> Resistive force theory is a lower order approximation compared with slender body theory but can be valid for describing isolated flagella as long as the drag from the attached cell body is not substantial.<sup>4</sup> It is widely used for modeling the dynamics of spermatozoa, which tend to have relatively small cell bodies and long flagella, and results have been shown to be consistent with experiments.<sup>5</sup> The simplicity of RFT has also been exploited in capturing the qualitative effects of fluid interactions where greater emphasis is placed on solving the elastic dynamics of the flagellum,<sup>6,7</sup> though it is also feasible to use SBT formulations for simulating flexible filaments in a fluid.<sup>8</sup>

Bacterial cell bodies tend to be much larger in relation to their flagella compared with spermatozoa. Since RFT does not accommodate long range hydrodynamic interactions, such as those between the cell body and flagellum, it is less suitable for models of bacterial propulsion. The canonical monotrichous bacterium, with a spherical or ellipsoidal cell body and rigidly rotating

---

<sup>a)</sup> Author to whom correspondence should be addressed. Electronic mail: [shum@maths.ox.ac.uk](mailto:shum@maths.ox.ac.uk). Present address: Department of Chemical and Petroleum Engineering, University of Pittsburgh, Pittsburgh, Pennsylvania 15261, USA.

helical flagellum, has been extensively studied with slender body theory<sup>9,10</sup> and boundary element methods (BEM),<sup>11–13</sup> which are based on the exact solution to the fluid flow problem given by the boundary integral equation. The immersed boundary method has also been effectively used to model fluid flows around single and multiple bacteria.<sup>14</sup> To justify the intensive computations, BEMs are best used in situations where the fluid boundary conditions must be treated with high precision, such as swimming very near a solid surface or another swimming cell. The former was described by Shum *et al.*<sup>13</sup> and Giacché *et al.*,<sup>15</sup> while the latter was considered by Ramia *et al.*<sup>12</sup> and Ishikawa *et al.*<sup>16</sup> Both of these situations are biologically relevant for swimming in microfluidic channels or porous media, and in biofilm initiation, where hydrodynamics can explain much of the phenomenon of boundary accumulation, which has important consequences for the impact of micro-organisms.

Mathematical predictions of bacteria swimming speeds in bulk fluid have been shown to agree reasonably well with experiment.<sup>17,18</sup> However, previous models do not take into account the mechanical properties of the flagellar filament and hook, which connects the filament to the motor embedded in the cell body. The hook is usually not modeled as a distinct structure, while the flagellum is generally treated either as a rigid structure or as a flexible string of particles using a bead–spring approach.

The hook and flagellum have differing mechanical properties due to the differences in composition. Qualitatively, observations of monotrichous bacteria indicate that the flagellum is stiff enough to maintain a stable helical structure during its rotation associated with steady swimming. For example, Armitage and Macnab<sup>19</sup> found through microscopy observations that the flagellum of *Rhodobacter sphaeroides* formed a linear helix of constant length for any given cell during its rotation. Flexural rigidity has been estimated for filaments of several bacterial species, such as *Escherichia coli*, based on balancing thermal and mechanical energy.<sup>20</sup> The flexural rigidity of filaments from *Vibrio alginolyticus*, a monotrichous species, was estimated at  $10 \text{ pN } \mu\text{m}^2$  by comparison of a theoretical Kirchhoff rod model with experiment.<sup>21</sup> This is similar to the figure of  $3.5 \text{ pN } \mu\text{m}^2$  suggested in Ref. 22 for the peritrichous *Salmonella typhimurium* and estimates of filament stiffness across all species are within a range of one or two orders of magnitude.

Calculations show that hooks are several orders of magnitude more flexible than filaments. In peritrichous bacteria, hook flexibility is necessary to allow the flagella to bend around the cell body and form a bundle for effective propulsion.<sup>23</sup> Although monotrichous bacteria do not need this flexibility to form flagellar bundles, a comparison shows that their hooks are a mere 2–3 times stiffer than those of peritrichous bacteria.<sup>24</sup> Hence, hook flexibility may still be influential in the dynamics of bacteria with a single, polar flagellum. This is evident from work on mutants that grow exceptionally long hooks, which consequently have lower flexural rigidity and diminished motility.<sup>25</sup> Further investigation is required as we currently do not fully understand the mechanical role that the hook plays in bacterial swimming.

Given the importance of bacterial motility and surface accumulation, for example, in biofilm initiation and motility in microdevices and porous media, we wish to explore the function and influence of the hook during swimming. We consider elastic dynamics based on naturally straight flagellar hooks, as found in *R. sphaeroides* and *V. alginolyticus*. Based on available data, flagellar filaments are much stiffer than hooks so most of the bending observed can be associated with deformations of the hook rather than the filament. We therefore incorporate elastic hook behaviour into our mathematical model while treating the filament as a rigid body as before.

Many theoretical studies of cilia and eukaryotic flagellar motion have given considerable attention to the elastic behaviour of the filament,<sup>26,27</sup> since active bending is the mechanism by which motion arises. In contrast, the bacterial flagellar filament and hook are passive and driven by a single proximal torque motor; hence, there is less need for elastodynamic considerations. Certain situations, such as flagellar bundling in peritrichous bacteria, do require flexibility and some authors have used bead–spring models to model this.<sup>28,29</sup> There is also much interest in helical and naturally straight elastic rods both in terms of static configurations and dynamics in a viscous environment.<sup>30–32</sup> We use a simple model based on Kirchhoff rod theory for the dynamics of the hook, which will be described in more detail in Sec. II. We then look at the motion of a bacterium with a flexible hook

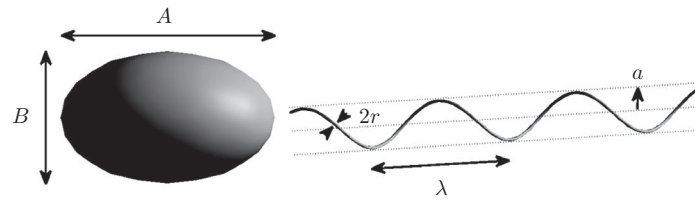


FIG. 1. Geometrical model of bacterial cell body and flagellum.

in bulk fluid and examine how accumulation near no-slip plane boundaries is affected by the hook dynamics. Results are followed by a discussion of biological implications.

## II. METHODS

### A. Geometrical modeling

The geometry of the bacterium influences the distribution of viscous stress and therefore its dynamics. The model is illustrated in Fig. 1. We represent the cell body with a prolate spheroid, as this resembles rod-shaped bacteria such as *R. sphaeroides*. The flagellum is a helical structure behind the cell body. The bacterial hook is a flexible coupling that transmits torque from the motor to the filament. In wild-type *R. sphaeroides*, the hook is roughly a cylindrical rod 100 nm long and 20 nm in diameter.<sup>33</sup> Hydrodynamically, it can be thought of as a small extension of the microns-long filament. Hence, we expect the hook to have limited hydrodynamic influence and we do not model the interaction of the hook with the fluid.

A very similar model was employed in the work of Shum *et al.*,<sup>13</sup> which we refer to as the rigid hook model. The difference is that previously the helical amplitude decayed smoothly to zero near the flagellum–cell body junction. This was effectively approximating the hook as a rigid, curved segment connecting the helical filament to the motor in the cell body. In the current work, the hook is allowed to bend, which means that the alignment between the flagellum and cell body is not necessarily constant. The two models are visually compared in Fig. 2. An important comment to make here is that we only consider naturally straight hooks, i.e., the hook is straight in its stress-free state. This is consistent with our understanding of the hook in the commonly investigated *R. sphaeroides* but many other species have naturally curved hooks, which could potentially affect swimming dynamics in those organisms.

### B. Equations of motion

At the microscopic scale of a swimming bacterium, the surrounding fluid satisfies the Stokes flow equations given the constitutive relation for an incompressible, viscous, Newtonian medium. Driven by a fixed motor torque, the swimmer moves with a translational velocity  $\mathbf{U}^B$  and rotational velocity  $\boldsymbol{\Omega}^B$  about the cell body–hook junction,  $\mathbf{x}^B$ . The flagellum shares this motion but has additional

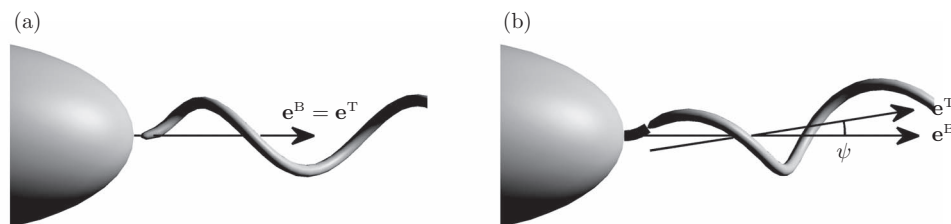


FIG. 2. Comparison between (a) the rigid hook model and (b) the current, flexible hook. The alignment angle between the body axis,  $\mathbf{e}^B$ , and the flagellum axis,  $\mathbf{e}^T$ , is denoted  $\psi$ . Since the shapes of the flagella differ near the cell body, the rigid model is not simply the limiting case where stiffness is taken to be very large in the flexible hook model.

degrees of freedom that govern its dynamics relative to the cell body: a translational velocity  $\mathbf{U}^T$  and a rotational velocity  $\boldsymbol{\Omega}^T$ . In order to determine these velocities, we use a boundary element method to compute the flow satisfying the required boundary conditions within the accuracy of the numerical scheme. The boundary integral equation for Stokes flow<sup>34</sup> reads

$$-\frac{1}{8\pi\mu} \int_{\text{B} \cup \text{T}} \mathbf{G}(\mathbf{x}^0, \mathbf{x}) \mathbf{f}(\mathbf{x}) dS(\mathbf{x}) = \mathbf{u}(\mathbf{x}^0) = \begin{cases} \mathbf{U}^B + \boldsymbol{\Omega}^B \wedge \tilde{\mathbf{x}}, & \mathbf{x}^0 \in \text{B} \\ (\mathbf{U}^B + \mathbf{U}^T) + (\boldsymbol{\Omega}^B + \boldsymbol{\Omega}^T) \wedge \tilde{\mathbf{x}}, & \mathbf{x}^0 \in \text{T} \end{cases}, \quad (1)$$

where  $\mu$  is the viscosity of the medium,  $\mathbf{G}$  is the second-rank Green's function tensor for Stokes flow in a three-dimensional domain,  $\mathbf{f}$  is the stress distribution on the surface of the bacterium, B is the surface of the body, T is the surface of the tail, and  $\tilde{\mathbf{x}} = (\mathbf{x}^0 - \mathbf{x}^B)$  is the position of a point on the bacterium relative to the body–hook junction. The Green's function is chosen either for an infinite fluid domain (free space) or for a fluid bounded by a no-slip plane wall (half space). Expressions for these forms are given by Blake.<sup>35</sup>

By considering the cell body and the flagellum as separate bodies in the fluid, we have the force and moment balance equations:

$$\left. \begin{aligned} \int_{\text{B}} \mathbf{f} dS + \mathbf{F}^B = \mathbf{0}, & \quad \int_{\text{B}} \tilde{\mathbf{x}} \wedge \mathbf{f} dS + \boldsymbol{\tau}^B = \mathbf{0}, \\ \int_{\text{T}} \mathbf{f} dS + \mathbf{F}^T = \mathbf{0}, & \quad \int_{\text{T}} \tilde{\mathbf{x}} \wedge \mathbf{f} dS + \boldsymbol{\tau}^T = \mathbf{0}, \end{aligned} \right\} \quad (2)$$

where  $\mathbf{F}^B$  and  $\boldsymbol{\tau}^B$  are the forces and moments exerted on the cell body by the hook and  $\mathbf{F}^T$  and  $\boldsymbol{\tau}^T$  are the forces and moments exerted on the flagellum by the hook.

We now describe a method for determining the mechanical body–hook and tail–hook interactions,  $\mathbf{F}^B$ ,  $\boldsymbol{\tau}^B$ ,  $\mathbf{F}^T$ , and  $\boldsymbol{\tau}^T$ , based on the elastic response of the connecting hook.

### C. The Kirchhoff hook model

The main model development described in this work is the inclusion of a flexible hook connecting the cell body to the rigid flagellar filament. The observed mechanical responses of the flagellum and hook are typically observed to be linear, excluding cases with the induction of large torsional deformations and the onset of polymorphic conformational changes, which are not considered here.<sup>22,36</sup> As we show in Appendix A, hook extension is unimportant. We therefore use the simplest inextensible, linearly elastic theory of rods with small strains but finite, three-dimensional centerline deformations. This is widely known as Kirchhoff rod theory,<sup>37–40</sup> which further assumes that the rod is unshearable. Based on physiological estimates of hook stiffness, it can be shown that a quasi-static description of the rod is appropriate at timescales comparable with the motor frequency. Furthermore, viscous stresses acting on the surface of the hook may be neglected. These two simplifications are also justified in Appendix A.

We now briefly summarize a general kinematic description of a directed curve, which will represent the centerline of a rod, and the constitutive relations for the Kirchhoff model.

The undeformed, or reference, curve is defined by a vector-valued function  $\mathbf{x}^0(s)$ , where the spatial parameter  $s$  can be taken as the arc length. For a finite curve of length  $L$ , we have the bounds  $0 \leq s \leq L$ . We define a set of right-handed, orthonormal local director vectors  $\{\mathbf{d}_i^0(s), i = 1, 2, 3\}$ . It is assumed that  $\mathbf{x}^0$  and  $\mathbf{d}_i^0$  vary smoothly with  $s$  but no additional specifications are necessary at this stage. At time  $t$ , the (possibly deformed) curve is given by  $\mathbf{x}(s, t)$ , where  $s$  is the arc length in the undeformed curve corresponding to the same material point, and the local directors are  $\{\mathbf{d}_i(s, t), i = 1, 2, 3\}$ . We require that these directors are twice differentiable functions of arc length and time and again form a right-handed, orthonormal basis.

For each  $s$  and  $t$  we can define a twist vector  $\boldsymbol{\kappa}(s, t) = \kappa_i(s, t)\mathbf{d}_i(s, t)$  and a spin vector  $\boldsymbol{\omega}(s, t)$  such that the kinematics of the curve are described by

$$\mathbf{d}'_i = \boldsymbol{\kappa} \wedge \mathbf{d}_i, \quad \dot{\mathbf{d}}_i = \boldsymbol{\omega} \wedge \mathbf{d}_i, \quad i = 1, 2, 3. \quad (3)$$

Throughout this article we will use the convention of summation over indices  $i = 1, 2, 3$  where they appear twice in the same term. We also use primes to signify derivatives with respect to arc length and dots to signify time derivatives.

A rod can be defined as a curve with finite thickness. We identify  $\mathbf{d}_1(s, t)$  and  $\mathbf{d}_2(s, t)$  with orthogonal orientations in the material cross section of the rod at arc length  $s$  and define the remaining director by  $\mathbf{d}_3 := \mathbf{d}_1 \wedge \mathbf{d}_2$ . The directors in the reference configuration are similarly defined. It is assumed that no two cross sections of the rod intersect one another whether in the reference or deformed configurations. The material point described by

$$\mathbf{X}^0(s, x_1, x_2) = \mathbf{x}^0(s) + x_1\mathbf{d}_1^0(s) + x_2\mathbf{d}_2^0(s) \quad (4)$$

in the reference configuration deforms to the position

$$\mathbf{X}(s, x_1, x_2, t) = \mathbf{x}(s, t) + \mathbf{r}(s, x_1, x_2, t), \quad (5)$$

where  $\mathbf{r}$  is a displacement from the centerline that depends on the original material position and the current deformation.

In the Kirchhoff model, it is assumed that the rod is inextensible and unsharable and that the cross sections of the undeformed rod are only rotated and translated upon deformation of the rod. The tangent vector is then given by  $\mathbf{v} = \mathbf{d}_3$  and the deformed directors track the deformation of the material lines marked by the directors in the reference configuration with the displacement vector of a material point from the centerline taking the simple form  $\mathbf{r}(s, x_1, x_2, t) = x_1\mathbf{d}_1(s, t) + x_2\mathbf{d}_2(s, t)$ . In fact, we will not make direct use of the last assumption except at the two ends of the rod, where we will assume that the cross sections at the two ends attach tangentially to the cell body and to the proximal tip of the flagellar filament, respectively. In other words, the hook protrudes perpendicularly from the cell body and joins with the flagellar filament with a continuous tangent along the centerline.

The stresses acting across each cross section of the rod lead to a net contact force  $\mathbf{n} = n_i\mathbf{d}_i$  and net contact moment  $\mathbf{m} = m_i\mathbf{d}_i$ . We use the convention that these quantities are exerted by the side with greater  $s$  on the side with smaller  $s$ . Neglecting inertia and viscous stresses, force and moment balance considerations on a vanishingly short section of the rod lead to the equations (see Antman<sup>40</sup> for more details)

$$\left. \begin{aligned} \mathbf{n}' &= \mathbf{0}, \\ \mathbf{m}' + \mathbf{d}_3 \wedge \mathbf{n} &= \mathbf{0}. \end{aligned} \right\} \quad (6)$$

We use a linear constitutive relation between the strain and the elastic moment in the rod. Assuming the rod is uniform and of circular cross section and has no finite preferred curvature or torsion, the moment can be expressed as

$$\mathbf{m} = EI(\kappa_1\mathbf{d}_1 + \kappa_2\mathbf{d}_2 + \Gamma\kappa_3\mathbf{d}_3), \quad (7)$$

where  $E$  is the Young's modulus of the material,  $I$  is the moment of inertia of the cross section, and  $\Gamma = GJ/EI$  is the ratio of twisting stiffness  $GJ$  to bending stiffness  $EI$ . Using this formula for the moment in (6), we find

$$\left. \begin{aligned} \kappa'_1 &= \frac{1}{EI}(\mathbf{n} \cdot \mathbf{d}_2) - \kappa_2\kappa_3(\Gamma - 1), \\ \kappa'_2 &= -\frac{1}{EI}(\mathbf{n} \cdot \mathbf{d}_1) + \kappa_1\kappa_3(\Gamma - 1), \\ \kappa'_3 &= 0. \end{aligned} \right\} \quad (8)$$

Treating the time  $t$  as a parameter, (8) and the equations for  $\mathbf{d}_i'$  in (3) yield a system of ordinary differential equations (ODEs) for  $\kappa(s, t)$ , and  $\mathbf{d}_i(s, t)$ ,  $i = 1, 2, 3$ . This system can be solved as an initial value problem in  $s$ . From (6), we see that the shear force does not vary with arc length, allowing us to write  $\mathbf{n}(s, t) = \mathbf{n}^B(t)$ , where we have defined the parameter  $\mathbf{n}^B(t) := \mathbf{n}(0, t)$ . We also require  $\mathbf{d}_i^B(t) := \mathbf{d}_i(0, t)$  and  $\kappa_i^B(t) := \kappa_i(0, t)$ , which we use as the initial values to determine  $\mathbf{d}_i(s, t)$  and  $\kappa_i(s, t)$  for  $0 \leq s \leq L$ . The system of ODEs is solved with the fourth-order Runge-Kutta method in our work. The rod shape is then constructed by integrating the tangent vector,  $\mathbf{x}' = \mathbf{d}_3$ . In Sec. II D, we will discuss a method of tracking the evolution of  $\mathbf{d}_i^B(t)$ ,  $\mathbf{n}^B(t)$ , and  $\mathbf{m}^B(t) := \mathbf{m}(0, t)$ , which is related to  $\kappa^B(t)$  by formula (7).

These elastic rod equations will be applied to the bacterial hook, which is of length  $L^H$ . Since we will mainly be concerned with the end points  $\mathbf{x}^B$  and  $\mathbf{x}^T$ , where the hook meets the cell body and flagellum, respectively, we summarize the solution to the rod equations symbolically as

$$\left. \begin{aligned} \mathbf{x}^T &= \mathbf{x}^B + \mathbf{X}(\mathbf{d}_1^B, \mathbf{d}_2^B, \mathbf{d}_3^B, \mathbf{n}^B, \mathbf{m}^B), \\ \mathbf{d}_1^T &= \mathbf{D}_1(\mathbf{d}_1^B, \mathbf{d}_2^B, \mathbf{d}_3^B, \mathbf{n}^B, \mathbf{m}^B), \\ \mathbf{d}_2^T &= \mathbf{D}_2(\mathbf{d}_1^B, \mathbf{d}_2^B, \mathbf{d}_3^B, \mathbf{n}^B, \mathbf{m}^B), \\ \mathbf{d}_3^T &= \mathbf{D}_3(\mathbf{d}_1^B, \mathbf{d}_2^B, \mathbf{d}_3^B, \mathbf{n}^B, \mathbf{m}^B), \\ \mathbf{m}^T &= \mathbf{M}(\mathbf{d}_1^B, \mathbf{d}_2^B, \mathbf{d}_3^B, \mathbf{n}^B, \mathbf{m}^B), \end{aligned} \right\} \quad (9)$$

where we have shortened notation by defining  $\mathbf{d}_i^T := \mathbf{d}_i(L^H, t)$  and  $\mathbf{m}^T := \mathbf{m}(L^H, t)$ . We set  $\mathbf{d}_3^B \equiv \mathbf{e}^B$  (see Fig. 2) while the initial choice of  $\mathbf{d}_1^B$  and  $\mathbf{d}_2^B$  is arbitrary within the constraints of orthonormality of the basis. The response functions  $\mathbf{X}$ ,  $\mathbf{D}_i$ , and  $\mathbf{M}$  depend on two intrinsic properties of the rod: the bend/twist ratio  $\Gamma$  and the relative hook rigidity,

$$k^H := \frac{EI}{\tau^M L^H}, \quad (10)$$

which we also refer to as the relative hook stiffness. We will see that the relative hook stiffness significantly influences the dynamics for the swimmer and it is worth bearing in mind that this ratio need not be constant. A bacterium with varying motor torque, either through regulation or as a result of environmental conditions, will have a time dependent relative hook stiffness.

#### D. Bacterial dynamics with hook response

The motion of the flagellum relative to the cell body is dictated by the changes in shape and orientation of the hook. If we write a point on the flagellum as

$$\mathbf{x}^0 = \mathbf{x}^T + y_i \mathbf{d}_i^T, \quad (11)$$

then, noting that  $\dot{y}_i = 0$  by the assumed rigid body behaviour of the flagellar filament, the instantaneous velocity at  $\mathbf{x}^0$  is given by

$$\begin{aligned} \mathbf{u}(\mathbf{x}^0) &= \dot{\mathbf{x}}^T + y_i \dot{\mathbf{d}}_i^T \\ &= \left( \dot{\mathbf{x}}^B + \boldsymbol{\omega}^B \wedge \mathbf{X} + \frac{\partial \mathbf{X}}{\partial \mathbf{n}^B} \times \dot{\mathbf{n}}^B + \frac{\partial \mathbf{X}}{\partial \mathbf{m}^B} \times \dot{\mathbf{m}}^B \right) + y_i \boldsymbol{\omega}^T \wedge \mathbf{d}_i^T, \end{aligned} \quad (12)$$

where  $\boldsymbol{\omega}^B = \boldsymbol{\omega}(0, t)$  is the spin vector at the body end of the hook. This is the sum of the cell body rotation vector and a spin rate around the motor axis, i.e.,  $\boldsymbol{\omega}^B = \boldsymbol{\Omega}^B + \omega^M \mathbf{e}^B$ . We also write  $\boldsymbol{\omega}^T = \boldsymbol{\omega}^B + \boldsymbol{\Omega}^H$ , where  $\boldsymbol{\Omega}^H$  is the spin vector of the flagellum end of the hook relative to the cell body end due to  $\dot{\mathbf{n}}^B$  and  $\dot{\mathbf{m}}^B$  satisfying

$$\frac{\partial \mathbf{D}_i}{\partial \mathbf{n}^B} \times \dot{\mathbf{n}}^B + \frac{\partial \mathbf{D}_i}{\partial \mathbf{m}^B} \times \dot{\mathbf{m}}^B = \boldsymbol{\Omega}^H \wedge \mathbf{D}_i, \quad i = 1, 2, 3. \quad (13)$$

Comparing (12) with the general form of the velocity on the flagellum in (1), we see that

$$\left. \begin{aligned} \mathbf{U}^T &= \frac{\partial \mathbf{X}}{\partial \mathbf{n}^B} \times \dot{\mathbf{n}}^B + \frac{\partial \mathbf{X}}{\partial \mathbf{m}^B} \times \dot{\mathbf{m}}^B + \boldsymbol{\Omega}^T \wedge (\mathbf{x}^B - \mathbf{x}^T), \\ \boldsymbol{\Omega}^T &= \omega^M \mathbf{e}^B + \boldsymbol{\Omega}^H. \end{aligned} \right\} \quad (14)$$

The partial derivatives,  $\partial \mathbf{X}/\partial \mathbf{n}^B$ ,  $\partial \mathbf{X}/\partial \mathbf{m}^B$ ,  $\partial \mathbf{D}_i/\partial \mathbf{n}^B$ , and  $\partial \mathbf{D}_i/\partial \mathbf{m}^B$ , can be computed using finite difference formulae. Noting (13), we can write  $\mathbf{U}^T$  and  $\boldsymbol{\Omega}^T$  as linear functions of the unknown velocities  $\dot{\mathbf{n}}^B$ ,  $\dot{\mathbf{m}}^B$ , and  $\omega^M$ .

Contact between the Kirchhoff hook and the cell body and between the hook and flagellar filament determines the relevant boundary conditions for all three structures. Relating the hydrodynamic force and torque constraints (2) to the boundary conditions on the hook, we find

$$\left. \begin{aligned} \mathbf{F}^B &= \mathbf{n}^B, & \boldsymbol{\tau}^B &= \mathbf{m}^B, \\ \mathbf{F}^T &= -\mathbf{n}^B, & \boldsymbol{\tau}^T &= -\mathbf{m}^T - (\mathbf{x}^T - \mathbf{x}^B) \wedge \mathbf{n}^B = -\mathbf{m}^B. \end{aligned} \right\} \quad (15)$$

To enforce a prescribed motor torque, we use the condition  $\mathbf{e}^B \cdot \boldsymbol{\tau}^B = -\tau^M$ , which is equivalent to the rod condition  $m_3^B = -\tau^M$ . The other components of torque and force are obtained by time stepping. At a given time  $t$ , we have the values of  $\mathbf{x}^B$ ,  $\mathbf{d}_i^B$ ,  $\mathbf{n}^B$ , and  $\mathbf{m}^B$ . From these we can compute the configuration of the hook and hence also of the flagellum.

For a BEM mesh with  $N$  collocation nodes, we have a system of  $3N$  boundary integral equations (1) and 12 balance considerations (2) at a given instant in time. We solve this to determine the unknowns:  $3N$  traction components on the surface mesh, 6 body velocities  $\mathbf{U}^B$  and  $\boldsymbol{\Omega}^B$ , 5 rates of change of hook force and moment  $\dot{\mathbf{n}}^B$ ,  $\dot{m}_1^B$ , and  $\dot{m}_2^B$ , and the motor frequency  $\omega^M$ . In total we have  $3N + 12$  unknowns and an equal number of equations, which we solve using the lower triangular-upper triangular decomposition technique with the LAPACK driver routine, DGESV. The meshes used in this study had about  $N = 550$  nodes, requiring  $\sim 2$  s to set up and solve the linear equations on a desktop personal computer. Simulating the dynamics over one motor revolution required 3–5 min.

## E. Steady states of the hook

We first restrict attention to swimming in unbounded fluid with an axisymmetric cell body so that the velocities in the reference frame of the hook are independent of the rotational phase of the body relative to the hook. In this reference frame, the velocities depend only on the instantaneous shape of the hook, i.e., we can write

$$\mathbf{v} = \mathcal{F}(\mathbf{n}^B, \mathbf{m}^B), \quad (16)$$

where  $\mathbf{v}$  can describe any of the velocities in the hook basis, such as the translational velocity of the swimmer, and  $\mathcal{F}$  is a function that we are able to numerically evaluate by solving the BEM problem. Consider the case where  $\mathbf{v}$  is the vector of time derivatives of the hook contact forces and moments. Then the roots of the function  $\mathcal{F}$  are the steady states of the hook,  $\mathbf{n}^{B*}$  and  $\mathbf{m}^{B*}$ . When the hook is in such a steady state, the flagellum simply rotates about the body axis. The stability of this state is given by the eigenvalues of the matrix of partial derivatives of  $\mathcal{F}$ . We denote the real part of the eigenvalue with the greatest real part by  $\Lambda$ . The steady state is stable if  $\Lambda < 0$  and unstable if  $\Lambda > 0$ .

We use Newton's method to find steady states. Convergence using this method usually requires a good initial estimate of  $\mathbf{n}^{B*}$  and  $\mathbf{m}^{B*}$ , which may be a known steady state of a similar swimmer or an estimate obtained by simulating the transient dynamics of the hook until an equilibrium is reached.

Once we have obtained a steady state for the hook, we can define the steady alignment angle,  $\psi^*$ , which is the constant angle between the body and flagellum axes at the steady hook configuration. We can also define the steady swimming speed,  $U^*$ , which is the mean speed of the swimmer on timescales much longer than a motor revolution. If the cell body is axisymmetric, the hook shape is steady and the swimmer is in free space, then the velocities are constant in the reference frame of the flagellum and the mean speed is given in terms of the instantaneous quantities,  $\mathbf{U}^B$ ,  $\boldsymbol{\Omega}^B$ , and



$\boldsymbol{\Omega}^T \equiv \omega^M \mathbf{e}^B$ , by the formula<sup>11</sup>

$$U^* = \mathbf{U}^B \cdot \frac{\boldsymbol{\Omega}^B + \boldsymbol{\Omega}^T}{\|\boldsymbol{\Omega}^B + \boldsymbol{\Omega}^T\|}. \quad (17)$$

## F. Tracking

The instantaneous configuration of the swimmer is described by  $\mathbf{x}^B$ ,  $\mathbf{e}^B$ ,  $\mathbf{e}^\perp$ ,  $\mathbf{n}^B$ ,  $\mathbf{m}^B$ , and  $\phi^H$ , where  $\mathbf{e}^\perp$  is a cell body orientation vector perpendicular to  $\mathbf{e}^B$ ,  $\phi^H$  is the phase of the hook director basis relative to the body orientation, and the other quantities are as previously defined. Solving the boundary integral equation with the constraints described above yields the instantaneous velocities,  $\mathbf{U}^B$ ,  $\boldsymbol{\Omega}^B$ ,  $\dot{\mathbf{n}}^B$ ,  $\dot{m}_1^B$ ,  $\dot{m}_2^B$ , and  $\omega^M$  (we have  $\dot{m}_3^B = 0$  since we prescribe a constant motor torque). These velocities are determined by the configuration and in turn determine the rate of change of the configuration, which therefore evolves as a system of ODEs.

In principle, the time stepping of the model bacterium configuration could be performed using the predictor–corrector method of Shum *et al.*<sup>13</sup> for rigid hook swimmers. However, the elastic dynamics of the hook introduces a very short timescale, making the system of equations stiff. In order to avoid using prohibitively short time steps, an implicit rule must be used for time stepping. For better stability, the backward Euler scheme is used to update  $\mathbf{n}^B(t)$ , while the second-order trapezoidal rule is used for the other variables. For a general variable  $x$  and velocity  $\dot{x}$ , these rules are given by

$$x(t + \delta t) = x(t) + \delta t \times \dot{x}(t + \delta t) \quad (\text{Backward Euler}), \quad (18)$$

$$x(t + \delta t) = x(t) + \delta t \times (\dot{x}(t) + \dot{x}(t + \delta t))/2 \quad (\text{Trapezoidal}). \quad (19)$$

The orientation vectors are analogously transformed according to

$$\mathbf{e}^\gamma(t + \delta t) = \mathbf{R}[\delta t \times (\boldsymbol{\Omega}^B(t) + \boldsymbol{\Omega}^B(t + \delta t))/2] \times \mathbf{e}^\gamma(t), \quad \gamma = B, \perp, \quad (20)$$

where  $\mathbf{R}[\mathbf{u}]$  is the rotation matrix for a rotation through the angle  $\|\mathbf{u}\|$  in the direction  $\mathbf{u}/\|\mathbf{u}\|$ . Newton's method is used to solve these implicit equations for the evolution of the swimmer configuration variables.

The first issue we will explore is the general behaviour of the hook while swimming in an unbounded fluid. We will then consider the problem of swimming near a plane boundary. Previous models with a rigid hook connection showed that many bacterial shapes lead to trapping of the swimmer at constant distances near the boundary. In this study, we examine how flexibility of the bacterial hook influences this boundary accumulation.

## III. RESULTS

Two bacterial shapes are used in the results we present here. One of these shapes,  $B$ , is based on parameters estimated for *R. sphaeroides*.<sup>41</sup> Parameter values and a visual comparison are given in Appendix B. When applied to swimmers using the rigid hook model, both of these shapes give rise to boundary accumulating behaviour near a no-slip plane boundary. Unless otherwise stated, results are based on simulations with shape  $A$ .

### A. Bend/twist ratio

The bend/twist ratio  $\Gamma$  determines the relative tendency for a structure to bend or twist. This ratio is also related to the Poisson ratio  $\nu$  by the formula  $\Gamma = 1/(1 + \nu)$ . In particular,  $\Gamma = 2/3$  corresponds to an incompressible material and  $\Gamma = 1$  means that there is no transverse strain when the material is stretched in one direction. Most familiar materials are characterized by bend/twist ratios between these values. However, simulations<sup>42</sup> of the hook structure have given an estimated value of  $\Gamma \approx 20$ . Our simulations showed negligible variations (no more than 0.002%) in the steady

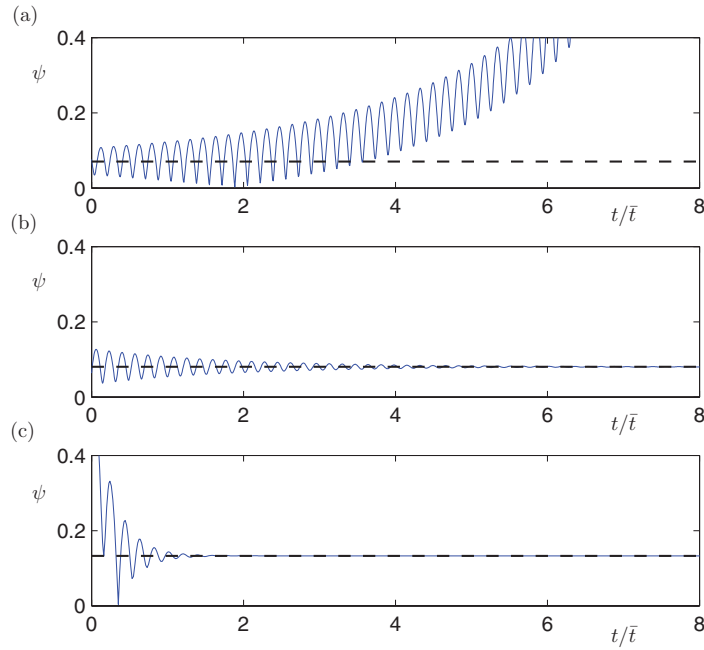


FIG. 3. Evolution of alignment angle  $\psi$  showing transient hook behaviour at different levels of relative stiffness. The steady state alignment angles are plotted as dashed lines (see Fig. 5). (a)  $k^H = 0.5$ , (b)  $k^H = 0.6$ , and (c)  $k^H = 1$ . Time is non-dimensionalized by the timescale  $\bar{\tau} = 16\pi^2\bar{a}^3\mu/\tau^M$ , where  $\bar{a}$  is the body's volumetric radius,  $\mu$  is the dynamic viscosity of the fluid, and  $\tau^M$  is the magnitude of the motor torque. The timescale corresponds to the period of revolution of a sphere of radius  $\bar{a}$  in the viscous fluid under the action of a torque of magnitude  $\tau^M$ .

state alignment angle and swimming speed while varying  $\Gamma$  from 0.5 to 32 for a constant relative hook stiffness  $k^H = 1$ . The insensitivity to  $\Gamma$  is to be expected since this parameter only affects the rate of twisting of the transverse hook directors about the centerline without altering the geometrical curvature. We use the value  $\Gamma = 1$  in all of the results presented.

## B. Hook rigidity

One of the outcomes observed in simulations in unbounded fluid is that the hook approaches a steady state, which is independent of the initial hook conditions. This corresponds to a hook of stable shape rotating with constant angular velocity about the motor axis, which leads to steady swimming. With a change in parameters, the alignment angle between the cell body and flagellum can oscillate and grow until the hook curvature becomes too large and beyond the scope of the current model. These two outcomes are illustrated in Fig. 3 and corresponding swimmers are shown at various times during a run in Fig. 4.

Using the method described above, we locate steady states and tracked the cell body–flagellum alignment angle, the mean swimming speed, and the stability of the steady state as the relative hook stiffness is gradually varied (Fig. 5). We find that below a critical value of relative hook stiffness  $k^H \approx 0.5$ , the steady state is unstable since  $\Lambda > 0$  (Fig. 5(b)). Diverging hook forces and torques lead to large deformations of the hook and the present Kirchhoff model can no longer be applied. In an intermediate range of relative hook stiffness, the flagellum is well aligned with the axis of the body and the swimming speed is close to that calculated for the corresponding bacterium in the rigid hook model.

For high values of relative stiffness, the hook is nearly straight. Since the hook joins tangentially to the helical flagellar filament and this tangent is not aligned with the axis of the helix, the flagellum rotates about an axis that is not close to its natural axis, causing significant oscillatory, lateral motion, and low net propulsion. A bifurcation is evidenced by a sharp jump in the stability measure,  $\Lambda$ , at  $k^H \approx 2$ , which coincides with the transition from the strong to the poor swimming regime. It should

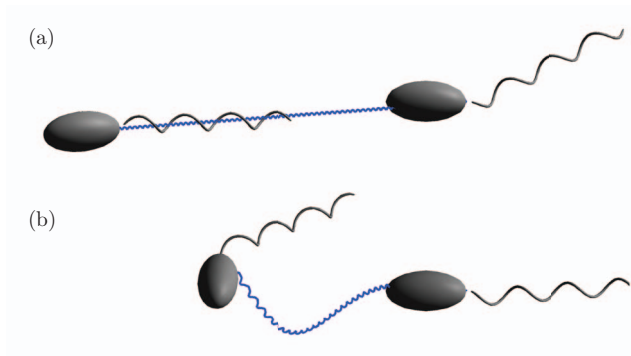


FIG. 4. Exemplar swimmers (a) with a stable hook state and (b) with an unstable steady hook state. The initial configurations (right) are out of equilibrium but a steady state is soon reached in the stable case. The curves between the two instances shown in each case trace the paths of the junction point  $\mathbf{x}^B$ . The trajectories correspond to cases (c) and (a), respectively, from Fig. 3 (enhanced online) [URL: <http://dx.doi.org/10.1063/1.4721416.1>] [URL: <http://dx.doi.org/10.1063/1.4721416.2>].

be emphasized that the limit of high relative stiffness does not correspond to the rigid hook model, which assumed an infinitely stiff but curved hook, allowing the helical axis to be aligned with the cell body axis.

Movies of swimming in the unstable ( $k^H = 0.5$ ), stable ( $k^H = 0.6$ ), and stable but inefficient ( $k^H = 2$ ) regimes are provided as videos to Figs. 4 and 5.

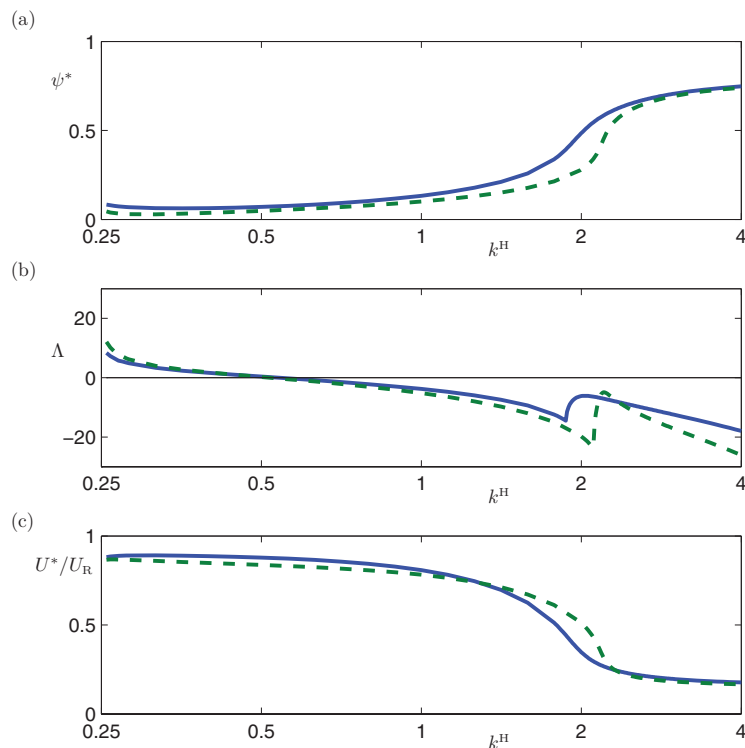


FIG. 5. Variations with relative hook stiffness of the steady state (a) alignment angle, (b) stability, and (c) swimming speed. Solid curves indicate data for bacterial shape *A* while dashed curves correspond to shape *B*. Swimming speeds in (c) are normalized by  $U_R$ , the speed computed using the rigid hook model with the equivalent geometrical parameters (enhanced online) [URL: <http://dx.doi.org/10.1063/1.4721416.3>].

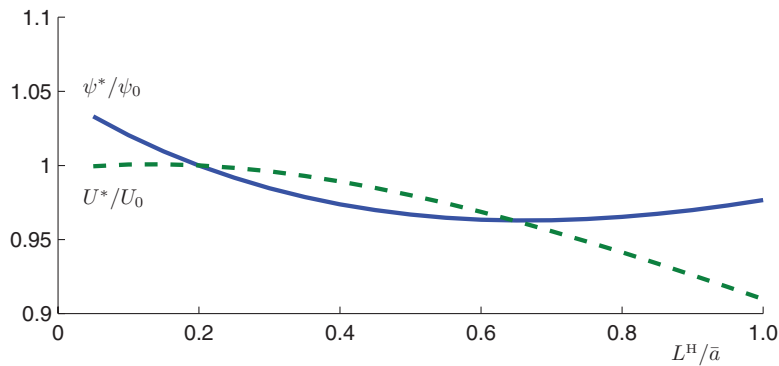


FIG. 6. Variations in steady state alignment angle (solid curve) and swimming speed (dashed curve) with hook length  $L^H/\bar{a}$ . The quantities are normalized by  $\psi_0$  and  $U_0$ , respectively, the values for the standard swimmer shape A, which has hook length  $L^H/\bar{a} = 0.2$ .

### C. Hook length

Increasing the hook length while maintaining a constant relative hook stiffness leads to gradual, but non-monotonic, changes in swimming speed and alignment angle (Fig. 6). Typical hook lengths range from about 50 nm in *E. coli*<sup>43</sup> to about 100 nm in *R. sphaeroides*.<sup>33</sup> We varied the simulated hook length from the equivalent of 35 nm to 700 nm and found that the free space swimming speed and cell body–flagellum alignment angle varied by no more than 10%. However, this does not imply that hook length regulation is unnecessary in bacteria since the hook relative rigidity,  $k^H := EI/\tau^M L^H$ , is inversely proportional to its length and we have shown that swimming motion is sensitive to relative hook rigidity.

### D. Boundary accumulation

Previous numerical studies have demonstrated the tendency for flagellated bacteria to swim in circular orbits near no-slip plane boundaries,<sup>13,15</sup> which we refer to as boundary accumulation. The path curvature is a result of the asymmetry in the vertical direction due to the horizontal wall. Both the stable swimming height and path curvature depend on the shape of the model swimmer and it was shown that not all swimmers achieve steady boundary swimming; some have a strong tendency to collide into the boundary and others are deflected away.

We now explore the effect of hook flexibility on near-surface swimming. In the presence of a plane boundary, the instantaneous swimmer dynamics depend on the distance and orientation relative to the wall as well as the hook forces and torques. Simulating over long timescales for particular values of relative hook stiffness, we observe a transient phase relaxing to periodic motion at a constant average distance from the wall, the defining feature of boundary accumulation (Fig. 7). In free space, the hook would approach a steady state, but the plane boundary breaks the invariance with respect to motor phase and we now find small oscillations in the hook shape on the timescale of the motor revolution.

However, other outcomes can be observed when the relative hook stiffness is varied. The boundary behaviour for bacterial shape A is summarized in Fig. 8. At an intermediate value of relative stiffness,  $k^H = 1$ , the flagellum is well aligned with the body, giving rise to behaviour very similar to that of an equivalent swimmer with the rigid hook model in both free space and half space fluid domains. Increasing the relative hook stiffness decreases the accumulation height slightly until we reach the critical point observed in free space at which the alignment angle becomes large and the swimmer begins to “wobble” significantly. This causes a much larger fluctuation in the junction position, which can be seen in Fig. 8, as well as a slightly increased average height above the wall.

Decreasing the relative hook stiffness from the intermediate value  $k^H = 1$ , we find that the stable accumulation height increases gradually before dropping suddenly at around  $k^H = 0.65$ . By  $k^H = 0.6$  we could no longer find a stable boundary accumulating trajectory as the swimmer had a

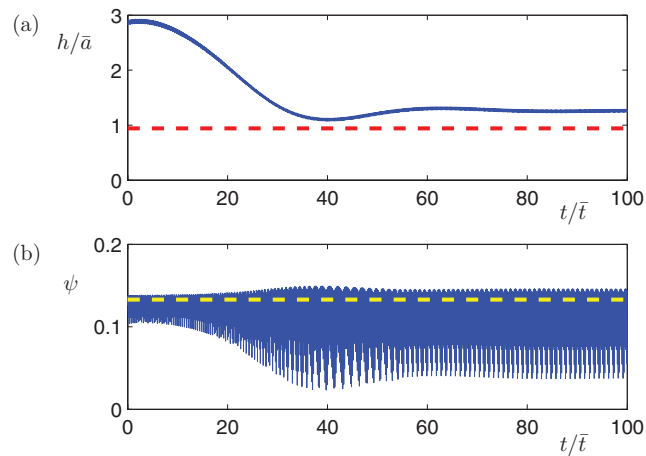


FIG. 7. Time series of (a) the swimmer's height above the wall,  $h$ , and (b) the hook alignment angle,  $\psi$ , as a bacterium with relative hook stiffness  $k^H = 1$  approaches a stable orbit above a plane boundary. The equivalent swimmer using the rigid hook model has a stable accumulation height  $h^*/\bar{a} \approx 0.94$ , indicated by a horizontal dashed line in (a) and the stable alignment angle  $\psi^* \approx 0.13$  in free space is marked by a horizontal dashed line in (b).

strong tendency to collide into the wall. Close to this critical relative stiffness, we note an increase in the alignment angle relative to the free space stable alignment. This is reminiscent of the loss of stability of the steady hook configuration seen in free space at around  $k^H = 0.5$  (Fig. 5). The wall appears to destabilize the hook by exerting additional stresses on the flagellum, causing the alignment angle to grow at relative hook stiffnesses slightly higher than the free space critical point.

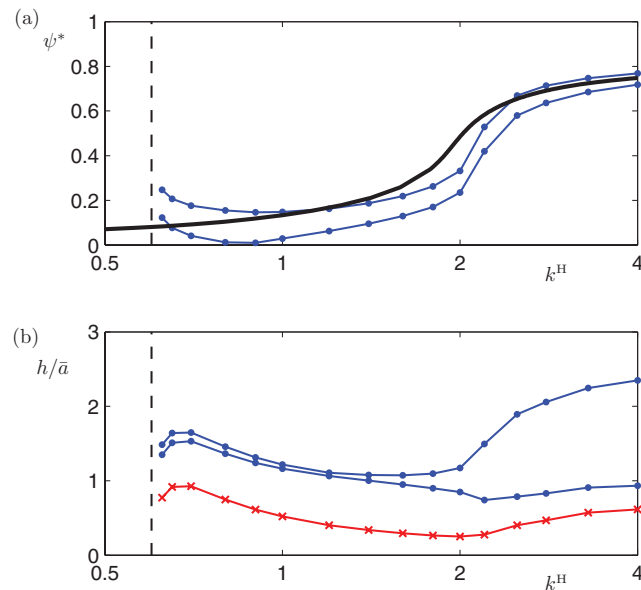


FIG. 8. Near-surface swimming behaviour after transience for bacterial shape *A* with varying relative hook stiffness. (a) Curves marked with dots indicate the minimum and maximum alignment angles attained over a cycle of periodic motion compared with the free space stable angle shown by the unmarked, thick curve. (b) The minimum and maximum swimming heights during stable boundary swimming (curves marked with dots) and the minimum separation distance between the wall and the swimmer (curve marked with crosses). Using the rigid hook model, this swimmer would have a stable swimming height of  $h^*/\bar{a} \approx 0.94$ . The dashed lines on the left hand side mark the relative stiffness value for which the swimmer was found to collide with the wall and no boundary accumulating trajectory could be obtained.

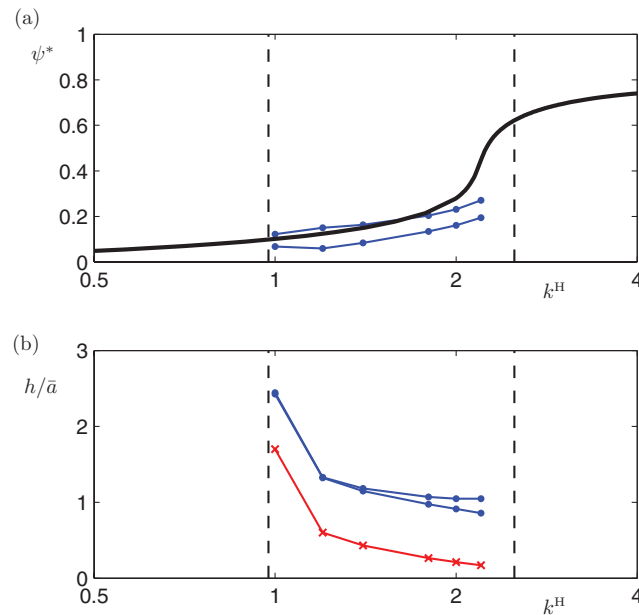


FIG. 9. Near-surface swimming behaviour after transience for bacterial shape  $B$  with varying relative hook stiffness. (a) Curves marked with dots indicate the minimum and maximum alignment angles attained over a cycle of periodic motion compared with the free space stable angle shown by the unmarked, thick curve. (b) The minimum and maximum swimming heights during stable boundary swimming (curves marked with dots) and the minimum separation distance between the wall and the swimmer (curve marked with crosses). Using the rigid hook model, this swimmer would have a stable swimming height of  $h^*/\bar{a} \approx 0.92$ . The dashed lines on the left and right hand sides mark relative stiffness values for which the swimmer was found to escape from the wall and no boundary accumulating trajectory could be obtained.

The trends described above as the relative hook stiffness is altered do not apply to swimmers of all shapes. Using bacterial shape  $B$ , stable orbits were found, though for a much narrower range in relative stiffness (Fig. 9). Throughout the intermediate range of relative stiffness, a similar trend to that with shape  $A$  was observed: the stable height increased with decreasing relative stiffness. However, the variation was very abrupt near  $k^H = 1$  and trajectories failed to remain close to the wall when values  $k^H \leq 0.975$  were applied. Similarly, trajectories consistently deflected away from the boundary when values  $k^H \geq 2.5$  were tested. In other words, the swimmer transitioned from a boundary accumulator at intermediate values of relative hook stiffness to a boundary escaper when the relative stiffness was either too low or too high. This contrasts with shape  $A$ , which collided with the boundary when the hook was too flexible and maintained stable near-surface orbits at intermediate and high values of relative hook stiffness within the investigated range.

Two examples of boundary accumulating trajectories for bacterial shape  $A$  are shown in Fig. 10. One swimmer has relative hook stiffness  $k^H = 0.7$ , which is close to the lower limit for stable boundary accumulation, and the other has relative stiffness  $k^H = 2$ , just at the onset of “wobbling” motion. In addition to the difference in accumulation height, we note significantly different curvatures of the circular paths resulting purely from the change in relative hook stiffness.

## IV. DISCUSSION

### A. Free space

While hook flexibility is clearly necessary in peritrichous bacteria, where many filaments must wrap around the cell body to join a flagellar bundle, it is not understood what role hook flexibility has in monotrichous species. Analysis of several species revealed that hooks from monotrichous and peritrichous bacteria have similar stiffnesses.<sup>24</sup> From the results we have shown, there may be a bounded range of relative hook stiffness relative to the product of the hook length and motor torque

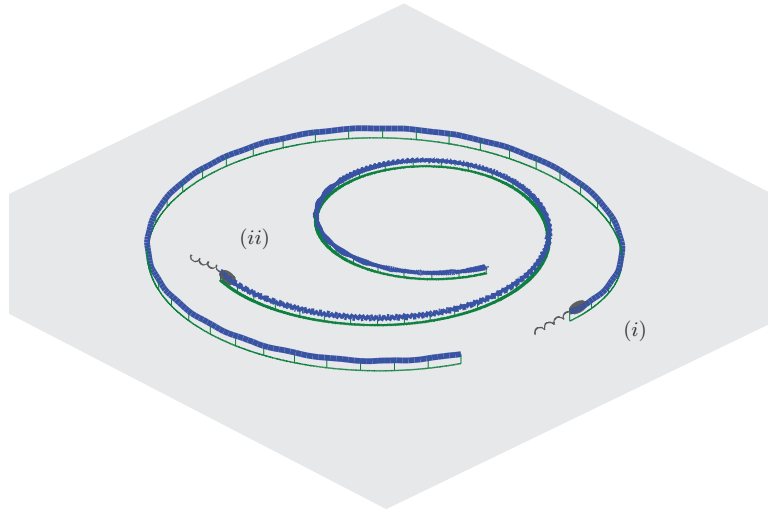


FIG. 10. Trajectories of two geometrically identical swimmers near plane boundaries. Swimmer (i) has relative hook stiffness  $k^H = 0.7$  and swimmer (ii) has relative hook stiffness  $k^H = 2$ . The 3D trajectories are shown in thick curves while projections of the trajectories onto the  $x$ - $y$  plane are shown in thin curves. The heights of the swimmers above the wall are also indicated at regular time intervals by vertical lines from the  $x$ - $y$  plane. The bacteria are shown at their respective starting positions. Note the much smaller radius of curvature of swimmer (ii) once the steady circular orbit is reached.

for good swimming performance. Using available empirical data, the physiological relative stiffness can be estimated at  $k^H \sim 0.1-1$ , the upper portion of which matches well with our computed regime of effective swimmers. However, comparisons must be made with care as comprehensive experimental data has not been collected for *R. sphaeroides* or any other suitable species. Since *R. sphaeroides* is known to have a number of distinct characteristics, including a naturally straight hook that our model assumes, it is possible that the elastic modulus and other important properties are significantly different from those of other species.

Using a modification of the method described in this article, one could examine the dynamics of bacteria with naturally curved hooks. Depending on the preferred curvature, there could be a much less restrictive upper bound on relative hook stiffness since body–flagellum alignment would require less deformation of the hook.

It has previously been noted that the motility of flagellated bacteria is sensitive to hook length. Mutants that grow abnormally long hooks have an impaired ability to swim.<sup>25</sup> We found only a modest variation in swimming behaviour with hook length for a fixed relative stiffness. However, relative hook stiffness is inversely proportional to hook length for a given material and our simulations indicated that stiffness has an important effect on flagellar motion. Lowering the relative stiffness was found to result in slightly higher swimming speeds, which seems to contradict empirical evidence. However, the dynamical instabilities that occur below a certain relative stiffness threshold provide a possible mechanical explanation for the need to regulate the hook length.

In an intermediate range of relative hook rigidity, there is little qualitative difference between the rigid hook model and the current model in unbounded fluid, where we find that the hook quickly enters a steady state and therefore becomes indistinguishable from rigid to an observer. The equations for the elastic rod determine the shape of the connecting hook so that the assumption of the growing helical amplitude of the filament in the rigid hook model is no longer required. Another difference is that the tail axis is not perfectly aligned with the body axis. This causes a slight “wobble” in the swimming motion of the bacterium, often also observed under a microscope, which is present to a much smaller degree in the rigid hook model.

## B. Accumulation at plane boundaries

Although the presence of a no-slip plane boundary does not appear to significantly perturb the hook state, we find that boundary accumulation is very sensitive to hook flexibility. Changes in relative hook rigidity can lead to abrupt transitions between colliding, stable boundary accumulating, and boundary escaping behaviour. Over the relative stiffness range that permits boundary accumulation, the stable swimming height varied between about  $h^*/\bar{a} = 1$  and  $h^*/\bar{a} = 1.5$  for shape *A* and from  $h^*/\bar{a} = 1$  to  $h^*/\bar{a} = 2.5$  for shape *B*.

Since  $h^*$  is measured from the wall to the cell body–hook junction, these variations in stable swimming height translate to minimum separations that vary from  $0.07\bar{a}$  to  $1.6\bar{a}$  as the relative stiffness is altered (Fig. 9). The lower figure amounts to about 50 nm, which, depending on the substrate, could make the bacterium susceptible to close range surface interactions. At the other end of the range,  $1.6\bar{a}$  is over 1  $\mu\text{m}$  for a bacterium like *R. sphaeroides*; the cell will be kept well beyond the reach of likely surface forces.

Thus, hook flexibility could alter the likelihood of close range surface interactions as well as the tendency to accumulate near surfaces at all. The changes in preferred separation also have a significant impact on the strength of hydrodynamic wall interactions and hence the radius of curvature of the circular orbit. This is evident in Fig. 10.

It has previously been shown that the cell body aspect ratio, flagellum length, and other parameters defining the bacterium's shape are important factors determining the swimming behaviour near boundaries. We now find that the relative hook stiffness can also affect the types of trajectories near boundaries. Indeed, it appears that the effects of varying the relative hook stiffness depend on the swimmer shape. Further investigation may shed light on the most important factors and general trends as shape and hook stiffness are altered.

## C. Adjusting the relative hook stiffness

We have discussed the influence of the relative hook stiffness on free space swimming and boundary accumulation. Such effects can be realized, at least theoretically, by changing the hook length or motor torque as well as the flexural rigidity. The motor torque can therefore potentially be controlled by changing the viscosity of the medium since this would affect the viscous load on the flagellum, leading to a different motor frequency and torque.<sup>44</sup>

It may also be possible to dynamically control the relative hook stiffness, and consequently boundary accumulation, by modulating the motor activity in a fixed medium. Most bacteria lack sufficient motor control to regulate boundary accumulation in this way but *R. sphaeroides* is known to have a variable-speed motor<sup>45</sup> so this effect may be physiologically relevant as well as being of possible interest to engineers of artificial flagellated micro-swimmers. Furthermore, the modulation of motor torque could result in substantial changes in the hook shape and dynamics, with the possibility of not only inducing boundary escape but also unpredictable reorientation, or tumbling, resulting from the elastic instability seen when the relative stiffness is sufficiently low. This would be an interesting area of further investigation.

## V. CONCLUSION

We have shown that within a limited range of hook rigidities relative to the product of the motor torque and hook length, a model bacterium with a single flagellum and naturally straight, elastic hook behaves in a manner that closely resembles the motion of model swimmers with curved, rigid hooks in unbounded fluid and near a plane boundary. This gives support for the use of simpler models that neglect hook dynamics as long as the hook stiffness of the modeled organism is in this regime and additional constraints, such as obstacles in the fluid, would not appreciably perturb the hook from its free space state.

At moderate relative hook rigidities in free space, the hook relaxes to a steady shape with the helical flagellum closely aligned with the body axis, resulting in effective propulsion. When the relative hook rigidity is increased beyond a critical level, there is a sudden misalignment between



the motor and flagellum axes, causing the swimmer to “wobble” inefficiently. Below a threshold relative stiffness, we found that the hook force and torque would suddenly undergo rapid changes characteristic of dynamical instabilities. The buckling of beams and rods has been extensively studied in other contexts<sup>30,32,46</sup> but is beyond the scope of the current study. However, it is likely that buckling and unsteady behaviour of the hook would be detrimental to effective swimming. We therefore conclude that monotrichous bacteria are unable to swim well if the hook is either too flexible or too rigid. Equivalently, our model predicts that effective swimming can only be achieved within a specific range of applied motor torques given a particular bacterium.

Although the boundary accumulation observed with rigid hook models can be reproduced with our Kirchhoff hook model, the behaviour that emerges is very sensitive to the relative stiffness of the hook. We have demonstrated that collisions, accumulation, and escape from boundaries can be induced by altering the relative hook stiffness, which has the implication that the behaviour of a bacterium near a plane boundary can be modulated by adjusting the motor activity.

Using the model we have developed, it would be interesting to address the problem of reverse swimming. Some species of marine bacteria, such as *V. alginolyticus*, frequently switch between backward and forward swimming.<sup>47</sup> Instead of simply retracing its path, it has been observed that the swimming direction changes by about 90° during the transitions from backward to forward swimming.<sup>48</sup> This process is not fully understood and may involve conformational changes of the flagellar filament itself. However, with the current model, we can examine the stability properties of the hook shape during backward swimming and simulate the orientation changes that occur when the motor torque is abruptly changed, assuming the filament does not deform. This also has relevance to the reorientation of *R. sphaeroides* as the motor stops and restarts.<sup>41</sup>

Another possible future application of our model is the investigation of tethered bacterium cells. Many past experiments involved rotating cells that are bound to a substrate by their flagellum filaments in order to determine mechanical properties of the flagellum.<sup>49–51</sup> Hashimoto *et al.*<sup>52</sup> recognized that complicated dynamics may arise from boundary interactions as the cells rotate. Although we have so far neglected short range cell–surface interactions, the boundary element method is well suited for simulating tethered cells and could be used to verify or propose corrections required for estimates of forces and torques in such systems.

## ACKNOWLEDGMENTS

We are grateful to Dr. George Wadhams and Professor Judy Armitage for insightful comments concerning the motility of *R. sphaeroides*.

## APPENDIX A: ROD APPROXIMATIONS

### 1. Inextensible

To show that hook extensibility is negligible, we estimate the deformation of an elastic rod supporting the compressive force required to push a bacterium-sized sphere of radius  $R = 1 \mu\text{m}$  through water at a physiological swimming speed  $U = 100 \mu\text{m s}^{-1}$ . The magnitude of the force is given by the Stokes drag formula,

$$F = 6\pi\mu RU \approx 2 \text{ pN}. \quad (\text{A1})$$

Based on bacterial hook properties, we suppose the rod has radius  $r = 10 \text{ nm}$ , length  $L^H = 100 \text{ nm}$ , and Young’s modulus  $E = 10^5 \text{ N m}^{-2}$ , with this last quantity estimated by simulation studies.<sup>42</sup> Powers<sup>53</sup> showed that the ratio of relaxation timescales for stretching and bending scaled with the square of the aspect ratio, that is,

$$T_{\text{stretch}}/T_{\text{bend}} \sim (r/L^H)^2 = 1/100 \ll 1. \quad (\text{A2})$$

We can therefore consider the equilibrium state of compression, where the strain is given by

$$\frac{\Delta L}{L^H} = \frac{F}{E\pi r^2} \approx 0.06. \quad (\text{A3})$$

This translates to a displacement of the flagellar filament of the order of 6 nm, which is negligible on the scale of the whole bacterium. The dominant influence of hook deformation on the swimmer is through the change in orientation of the flagellar filament relative to the cell body resulting from bending motion of the hook.

## 2. Quasi-static

For small, inextensible, planar deformations of the hook, we describe the dynamics with the Euler-Bernoulli beam equation,

$$\frac{\partial^2}{\partial x^2} \left( EI \frac{\partial^2 y}{\partial x^2} \right) + \rho A \frac{\partial^2 y}{\partial t^2} = f(x, t), \quad (\text{A4})$$

where  $x$  is the axis of the undeformed beam,  $y$  is the transverse deflection,  $E$  is the Young's modulus of the beam,  $I$  is the second moment of area,  $\rho$  is the mass density,  $A$  is the cross-sectional area, and  $f$  is the shear load per unit length along the beam.

For a cylinder of radius  $r = 10$  nm, the second moment of area is  $I = \pi r^4 / 4 \approx 10^{-32} \text{ m}^4$ . Assuming that both the deflection and the lengthscale of variations are of the order of the hook length, the elastic term in (A4) is of the magnitude

$$EI \frac{\partial^4 y}{\partial x^4} \sim EI(1/L^H)^3 \approx 10^{-6} \text{ N m}^{-1}. \quad (\text{A5})$$

Assuming that the hook is of the same density as water, we have  $\rho = 1000 \text{ kg m}^{-3}$ . The inertial term in (A4) is given by

$$\rho A \frac{\partial^2 y}{\partial t^2} \sim \rho \pi r^2 L^H / T^2 \approx 3 \times 10^{-20} / T^2 \text{ N m}^{-1}, \quad (\text{A6})$$

where  $T$  is the characteristic timescale of fluctuations. Bacteria typically swim with motor frequencies of 100–1000 Hz, giving a timescale of  $T \sim 10^{-3} - 10^{-2}$  s. This results in an inertial contribution of the order of  $10^{-16} - 10^{-14} \text{ N m}^{-1}$ . Comparing this with the elastic bending term, we conclude that inertia may be neglected.

## 3. No drag on hook

The shape of the hook is found by repeated integration of the quasi-static Euler-Bernoulli beam equation. On integrating once, we find the elastic bending force in terms of the contact and applied forces:

$$F(x) = EI \frac{\partial^3 y}{\partial x^3} = F_0 + \int_0^x f(s) ds. \quad (\text{A7})$$

Here,  $F_0$  is the contact force applied at the  $x = 0$  boundary of the hook, which we define to be the end attached to the flagellar filament, and the distributed load per unit length on the hook,  $f$ , is due to the action of viscous drag. In particular, noting the forces for the hook and flagellar filament will scale with their respective lengths and velocities, and given that the velocities are broadly the same, we anticipate the ratio



$$\frac{\int_0^{L^H} f(s) ds}{F_0} \sim \frac{L^H}{L_{\text{filament}}} \ll 1. \quad (\text{A8})$$

Therefore, we can neglect the influence of the viscous drag on the hook,  $f$ , and determine the shape of the hook by considering quasi-static elastic equations with no distributed load.

## APPENDIX B: BACTERIAL GEOMETRY PARAMETERS

The two sets of parameters for bacterial geometry used in the presented results are given in Table I. Shape *B* is based on parameters estimated for *R. sphaeroides*.<sup>41</sup>

TABLE I. Key parameters determining geometry of the model bacteria used in this article. The lengthscale  $\bar{a}$  is the volumetric radius of the spheroidal cell body.

Shape		
Body:		
Length/width	2.000	1.625
Hook:		
Length/ $\bar{a}$	0.200	0.213
Flagellum:		
Length/ $\bar{a}$	10.000	7.434
Radius/ $\bar{a}$	0.050	0.021
Pitch/ $\bar{a}$	2.000	1.770
Amplitude/ $\bar{a}$	0.318	0.276

- <sup>1</sup>G. Taylor, "Analysis of the swimming of microscopic organisms," *Proc. R. Soc. London, Ser. A* **209**, 447–461 (1951).
- <sup>2</sup>J. Gray, and G. J. Hancock, "The propulsion of sea-urchin spermatozoa," *J. Exp. Biol.* **32**, 802–814 (1955).
- <sup>3</sup>G. J. Hancock, "The self-propulsion of microscopic organisms through liquids," *Proc. R. Soc. London, Ser. A* **217**, 96–121 (1953).
- <sup>4</sup>R. E. Johnson and C. J. Brokaw, "Flagellar hydrodynamics. A comparison between resistive-force theory and slender-body theory," *Biophys. J.* **25**, 113–127 (1979).
- <sup>5</sup>B. M. Friedrich, I. H. Riedel-Kruse, J. Howard, and F. Jülicher, "High-precision tracking of sperm swimming fine structure provides strong test of resistive force theory," *J. Exp. Biol.* **213**, 1226–1234 (2010).
- <sup>6</sup>A. Hilfinger, A. K. Chattopadhyay, and F. Jülicher, "Nonlinear dynamics of cilia and flagella," *Phys. Rev. E* **79**, 051918 (2009).
- <sup>7</sup>H. Gadêlha, E. A. Gaffney, D. J. Smith, and J. C. Kirkman-Brown, "Nonlinear instability in flagellar dynamics: A novel modulation mechanism in sperm migration?" *J. R. Soc., Interface* **7**, 1689–1697 (2010).
- <sup>8</sup>A.-K. Tornberg and M. J. Shelley, "Simulating the dynamics and interactions of flexible fibers in Stokes flows," *J. Comput. Phys.* **196**, 8–40 (2004).
- <sup>9</sup>J. J. L. Higdon, "The hydrodynamics of flagellar propulsion: Helical waves," *J. Fluid Mech.* **94**, 331–351 (1979).
- <sup>10</sup>R. E. Johnson, "An improved slender-body theory for Stokes flow," *J. Fluid Mech.* **99**, 411–431 (1980).
- <sup>11</sup>N. Phan-Thien, T. Tran-Cong, and M. Ramia, "A boundary-element analysis of flagellar propulsion," *J. Fluid Mech.* **184**, 533–549 (1987).
- <sup>12</sup>M. Ramia, D. L. Tullock, and N. Phan-Thien, "The role of hydrodynamic interaction in the locomotion of microorganisms," *Biophys. J.* **65**, 755–778 (1993).
- <sup>13</sup>H. Shum, E. A. Gaffney, and D. J. Smith, "Modelling bacterial behaviour close to a no-slip plane boundary: The influence of bacterial geometry," *Proc. R. Soc. London, Ser. A* **466**, 1725–1748 (2010).
- <sup>14</sup>C.-Y. Hsu and R. Dillon, "A 3D motile rod-shaped monotrichous bacterial model," *Bull. Math. Biol.* **71**, 1228–1263 (2009).
- <sup>15</sup>D. Giacché, T. Ishikawa, and T. Yamaguchi, "Hydrodynamic entrapment of bacteria swimming near a solid surface," *Phys. Rev. E* **82**, 056309 (2010).
- <sup>16</sup>T. Ishikawa, G. Sekiya, Y. Imai, and T. Yamaguchi, "Hydrodynamic interactions between two swimming bacteria," *Biophys. J.* **93**, 2217–2225 (2007).
- <sup>17</sup>T. Goto, S. Masuda, K. Terada, and Y. Takano, "Comparison between observation and boundary element analysis of bacterium swimming motion," *JSME Int. J., Ser. C* **44**, 958–963 (2001).
- <sup>18</sup>S. Chattopadhyay and X.-L. Wu, "The effect of long-range hydrodynamic interaction on the swimming of a single bacterium," *Biophys. J.* **96**, 2023–2028 (2009).
- <sup>19</sup>J. P. Armitage and R. M. Macnab, "Unidirectional, intermittent rotation of the flagellum of *Rhodobacter sphaeroides*," *J. Bacteriol.* **169**, 514–518 (1987).
- <sup>20</sup>S. Trachtenberg and I. Hammel, "The rigidity of bacterial flagellar filaments and its relation to filament polymorphism," *J. Struct. Biol.* **109**, 18–27 (1992).
- <sup>21</sup>Y. Takano and T. Goto, "Numerical analysis of small deformation of flexible helical flagellum of swimming bacteria," *JSME Int. J., Ser. C* **46**, 1234–1240 (2003).
- <sup>22</sup>N. C. Darnton and H. C. Berg, "Force-extension measurements on bacterial flagella: Triggering polymorphic transformations," *Biophys. J.* **92**, 2230–2236 (2007).
- <sup>23</sup>H. C. Berg and R. A. Anderson, "Bacteria swim by rotating their flagellar filaments," *Nature (London)* **245**, 380–382 (1973).
- <sup>24</sup>A. Sen, R. K. Nandy, and A. N. Ghosh, "Elasticity of flagellar hooks," *J. Electron Microsc.* **53**, 305–309 (2004).

- <sup>25</sup> A. W. Williams, S. Yamaguchi, F. Togashi, S. I. Aizawa, I. Kawagishi, and R. M. Macnab, "Mutations in *fliK* and *fliH* affecting flagellar hook and filament assembly in *Salmonella typhimurium*," *J. Bacteriol.* **178**, 2960–2970 (1996).
- <sup>26</sup> M. Hines and J. J. Blum, "Bend propagation in flagella. I. Derivation of equations of motion and their simulation," *Biophys. J.* **23**, 41–57 (1978).
- <sup>27</sup> R. H. Dillon, L. J. Fauci, C. Omoto, and X. Yang, "Fluid dynamic models of flagellar and ciliary beating," *Ann. N. Y. Acad. Sci.* **1101**, 494–505 (2007).
- <sup>28</sup> H. Flores, E. Lobaton, S. Mendez-Diez, S. Tlupova, and R. Cortez, "A study of bacterial flagellar bundling," *Bull. Math. Biol.* **67**, 137–168 (2005).
- <sup>29</sup> N. Watari and R. G. Larson, "The hydrodynamics of a run-and-tumble bacterium propelled by polymorphic helical flagella," *Biophys. J.* **98**, 12–17 (2010).
- <sup>30</sup> A. Goriely and M. Tabor, "Nonlinear dynamics of filaments I. Dynamical instabilities," *Phys. D: Nonlinear Phenom.* **105**, 20–44 (1997).
- <sup>31</sup> R. E. Goldstein, T. R. Powers, and C. H. Wiggins, "Viscous nonlinear dynamics of twist and writhe," *Phys. Rev. Lett.* **80**, 5232–5235 (1998).
- <sup>32</sup> C. W. Wolgemuth, T. R. Powers, and R. E. Goldstein, "Twirling and whirling: Viscous dynamics of rotating elastic filaments," *Phys. Rev. Lett.* **84**, 1623–1626 (2000).
- <sup>33</sup> B. González-Pedrajo, T. Ballado, A. Campos, R. E. Sockett, L. Camarena, and G. Dreyfus, "Structural and genetic analysis of a mutant of *Rhodobacter sphaeroides* WS8 deficient in hook length control," *J. Bacteriol.* **179**, 6581–6588 (1997).
- <sup>34</sup> C. Pozrikidis, *Boundary Integral and Singularity Methods for Linearized Viscous Flow* (Cambridge University Press, New York, 1992).
- <sup>35</sup> J. R. Blake, "A note on the image system for a stokeslet in a no-slip boundary," *Proc. Cambridge Philos. Soc.* **70**, 303–310 (1971).
- <sup>36</sup> S. M. Block, D. F. Blair, and H. C. Berg, "Compliance of bacterial polyhooks measured with optical tweezers," *Cytometry* **12**, 492–496 (1991).
- <sup>37</sup> G. Kirchhoff, "Über das Gleichgewicht und die Bewegung eines unendlich dünnen elastischen Stabes," *J. Reine Angew. Math.* **1859**, 285–313 (1859).
- <sup>38</sup> G. R. Kirchhoff, *Vorlesungen über Mathematische Physik. Mechanik* (BG Teubner, Leipzig, 1876), Vol. 28.
- <sup>39</sup> E. H. Dill, "Kirchhoff's theory of rods," *Arch. Hist. Exact Sci.* **44**, 1–23 (1992).
- <sup>40</sup> S. S. Antman, *Nonlinear Problems of Elasticity* (Springer, New York, 2005).
- <sup>41</sup> J. P. Armitage, T. P. Pitta, M. A.-S. Vigeant, H. L. Packer, and R. M. Ford, "Transformations in flagellar structure of *Rhodobacter sphaeroides* and possible relationship to changes in swimming speed," *J. Bacteriol.* **181**, 4825–4833 (1999).
- <sup>42</sup> T. C. Flynn and J. Ma, "Theoretical analysis of twist/bend ratio and mechanical moduli of bacterial flagellar hook and filament," *Biophys. J.* **86**, 3204–3210 (2004).
- <sup>43</sup> M. L. DePamphilis and J. Adler, "Fine structure and isolation of the hook-basal body complex of flagella from *Escherichia coli* and *Bacillus subtilis*," *J. Bacteriol.* **105**, 384–395 (1971).
- <sup>44</sup> Y. Sowa and R. M. Berry, "Bacterial flagellar motor," *Q. Rev. Biophys.* **41**, 103–132 (2008).
- <sup>45</sup> H. L. Packer, H. Lawther, and J. P. Armitage, "The *Rhodobacter sphaeroides* flagellar motor is a variable-speed rotor," *FEBS Lett.* **409**, 37–40 (1997).
- <sup>46</sup> G. H. M. van der Heijden, S. Neukirch, V. G. A. Goss, and J. M. T. Thompson, "Instability and self-contact phenomena in the writhing of clamped rods," *Int. J. Mech. Sci.* **45**, 161–196 (2003).
- <sup>47</sup> S. Kudo, N. Imai, M. Nishitoba, S. Sugiyama, and Y. Magariyama, "Asymmetric swimming pattern of *Vibrio alginolyticus* cells with single polar flagella," *FEMS Microbiol. Lett.* **242**, 221–225 (2005).
- <sup>48</sup> L. Xie, T. Altindal, S. Chattopadhyay, and X.-L. Wu, "Bacterial flagellum as a propeller and as a rudder for efficient chemotaxis," *Proc. Natl. Acad. Sci. U.S.A.* **108**, 2246–2251 (2011).
- <sup>49</sup> S. M. Block, D. F. Blair, and H. C. Berg, "Compliance of bacterial flagella measured with optical tweezers," *Nature (London)* **338**, 514–518 (1989).
- <sup>50</sup> H. C. Berg and L. Turner, "Torque generated by the flagellar motor of *Escherichia coli*," *Biophys. J.* **65**, 2201–2216 (1993).
- <sup>51</sup> R. M. Berry, L. Turner, and H. C. Berg, "Mechanical limits of bacterial flagellar motors probed by electrorotation," *Biophys. J.* **69**, 280–286 (1995).
- <sup>52</sup> M. Hashimoto, T. Mashimo, T. Hirano, S. Yamaguchi, and S.-I. Aizawa, "Functional roles of the hook in a rotating tethered cell," *J. Mol. Biol.* **375**, 367–375 (2008).
- <sup>53</sup> T. R. Powers, "Dynamics of filaments and membranes in a viscous fluid," *Rev. Mod. Phys.* **82**, 1607–1631 (2010).